Supplemental Material for Dissipative superradiant spin amplifier for enhanced quantum sensing

Martin Koppenhöfer[1*], Peter Groszkowski[1], Hoi-Kwan Lau[2], and A. A. Clerk[1]
[1] *Pritzker School of Molecular Engineering, University of Chicago, Chicago, IL, USA*
[2] *Department of Physics, Simon Fraser University, Burnaby, BC, Canada*
[*] *To whom correspondence should be addressed; E-mail: koppenhoefer@uchicago.edu*
(Dated: July 10, 2022)

I. HEURISTIC ARGUMENT ON ADDED NOISE

In this section, we adapt Caves' derivation of the quantum limit on the added noise of a bosonic linear amplifier [1] to the phase-preserving spin amplifier considered in this work. We start by writing down a minimal description (in terms of Heisenberg equations of motion) of a spin amplifier that amplifies any polarization transverse to the z direction. The amplification process translates an input state (as encoded in the initial-time $t = 0$ collective spin operators $\hat{S}_\alpha \equiv \hat{S}_\alpha(0)$ for $\alpha \in \{x, y, z\}$), to an output state (similarly encoded in the final time $t = T$ Heisenberg-picture spin operators $\hat{S}_\alpha(T) \equiv \hat{T}_\alpha$). Assuming linear amplification dynamics suggests writing the the solution of the Heisenberg equations of motion in the form:

$$\hat{T}_x = G(T)\hat{S}_x + \hat{F}_x \ , \tag{1}$$

$$\hat{T}_y = G(T)\hat{S}_y + \hat{F}_y \ . \tag{2}$$

The first term in each equation captures the linear amplification dynamics, with $G(T)$ denoting the gain. The remaining Hermitian operators $\hat{F}_\alpha$ describe all additional terms arising from solving the Heisenberg equations. Note that at this stage, we do not make any assumptions about the dynamics of $\hat{S}_z$ and the value of $\hat{S}_z(T) \equiv \hat{T}_z$.

We next *assume* that the average values of the final-time spin operators are fully described by the linear gain terms (e.g. as is seen in our system for initial states with small transverse polarizations). As such, the $\hat{F}_\alpha$ can be viewed as zero-mean operators that describe added noise associated with the amplification dynamics. We further assume that these noise operators are uncorrelated with the initial spin state, i.e., $\langle \hat{S}_\alpha \hat{F}_\beta \rangle = 0$ and $[\hat{S}_\alpha, \hat{F}_\beta] = 0$. In reality, the $\hat{F}_\alpha$ also describe the nonlinear response of our system; we are implicitly assuming that the initial state of our system lets us safely ignore such terms (i.e., the initial transverse polarization is small).

With these assumptions in hand, we can now construct a bound on the size of the added noise. We first use the fact that the final-time spin operators must obey canonical spin commutation relations, and hence we must have $[\hat{T}_x, \hat{T}_y] = i\hat{T}_z$. This results in the constraint

$$\hat{T}_z = G^2(T)\hat{S}_z - i[\hat{F}_x, \hat{F}_y] \ . \tag{3}$$

The fluctuations in the final-time transverse spin operators are given by:

$$(\mathbf{\Delta} T_{x,y})^2 \equiv \langle \hat{T}^2_{x,y} \rangle - \langle \hat{T}_{x,y} \rangle^2 = G^2(T)(\mathbf{\Delta} S_{x,y})^2 + \langle \hat{F}^2_{x,y} \rangle \ . \tag{4}$$

Since the amplifier acts identically on the x and y components, $\langle \hat{F}^2_x \rangle$ and $\langle \hat{F}^2_y \rangle$ are identical and we can write

$$\begin{aligned} \langle \hat{F}^2_{x,y} \rangle &= \frac{1}{4}\langle \{\hat{F}_+, \hat{F}_-\} \rangle \geq \frac{1}{4}|\langle [\hat{F}_+, \hat{F}_-] \rangle| \\ &= \frac{1}{2}|\langle [\hat{F}_x, \hat{F}_y] \rangle| = \frac{1}{2}|[G^2(T)\langle \hat{S}_z \rangle - \langle \hat{T}_z \rangle]| \ , \end{aligned} \tag{5}$$

where we defined $\hat{F}_\pm = \hat{F}_x \pm i\hat{F}_y$ and used Eq. (3) in the last step. Using $|\partial_\phi \langle \hat{T}_{x,y} \rangle| = G(T)|\partial_\phi \langle \hat{S}_{x,y} \rangle|$, we thus find

$$\frac{(\mathbf{\Delta} T_{x,y})^2}{|\partial_\phi \langle \hat{T}_{x,y} \rangle|^2} \geq \frac{(\mathbf{\Delta} S_{x,y})^2}{|\partial_\phi \langle \hat{S}_{x,y} \rangle|^2} + \frac{1}{2G^2(T)} \frac{|G^2(T)\langle \hat{S}_z \rangle - \langle \hat{T}_z \rangle|}{|\partial_\phi \langle \hat{S}_{x,y} \rangle|^2} \ . \tag{6}$$

In our specific spin amplification protocol, we start with a CSS close to a maximally polarized state, i.e., $\langle \hat{S}_z \rangle = 2(\mathbf{\Delta} S_{x,y})^2 = N/2$, and we interrupt the amplification dynamics at the time $T = t_{\max}$ when the condition $\langle \hat{T}_z \rangle = 1/2$ holds. This yields

$$\frac{(\mathbf{\Delta} T_{x,y})^2}{|\partial_\phi \langle \hat{T}_{x,y} \rangle|^2} \geq \frac{1}{N}\left[2 - \frac{1}{G^2(T)N}\right] \ , \tag{7}$$

i.e., the spin amplification process doubles the input spin-projection noise in the large-N limit.

Note that this argument is *not* a strict theoretical lower bound on the noise that is added during the amplification step. Instead, it is a heuristic argument that helps one to develop a sense how much added noise can be expected due to amplification. Even though our amplification scheme is conceptually very simple, we numerically find that it does not saturate the prediction of this heuristic argument (see Figs. 3(b) of the main text and Fig. 5). Hence, an interesting question for future research is to refine this argument to see if the actual lower bound on the added noise in the large-N limit is larger than predicted here.

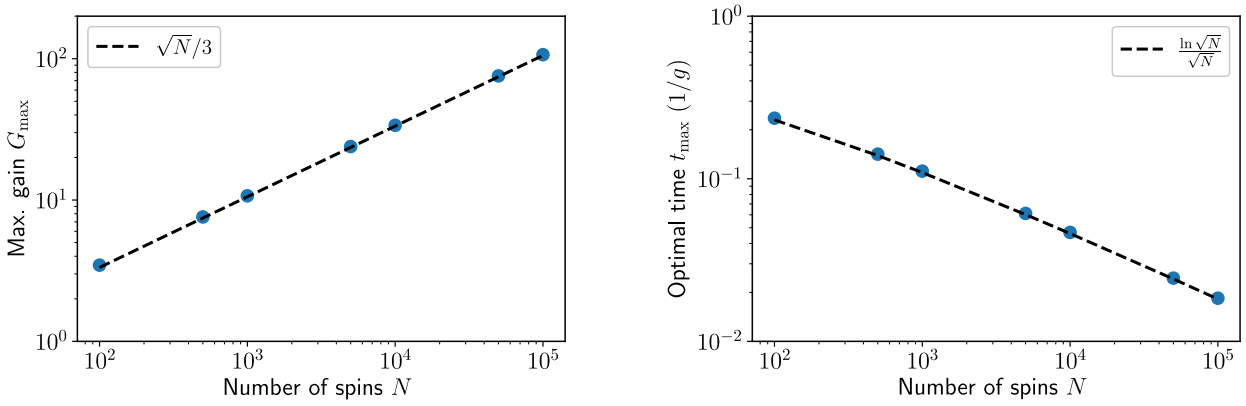

(a) (b)

FIG. 1. Mean-field theory analysis of the coherent amplification protocol (i.e., in the limit of an undamped cavity). Scaling of **(a)** the maximum gain $G_{\max}$ and **(b)** the corresponding time $t_{\max}$ as a function of spin number N. Results have been obtained by numerical solution of the MFT equations (10) to (21). Blue dots correspond to simulation data, while dashed black lines show the respective scaling behavior.

II. ADDITIONAL DETAILS ON THE DISSIPATIVE AMPLIFICATION PROTOCOL

A. Signal-dependence of the amplification time and dynamic range

In this section, we discuss the dependence of the amplification tiem $t_{\max}$ and the maximum gain $G_{\max}$ on the initial tilt angle ϕ, and we provide additional information on the dynamic range of the spin amplifier.

If all N spins are initialized in the excited state, (quantum) fluctuations will seed the superradiant decay towards the collective ground state. If the initialization to the excited state is imperfect but the deviation of the collective spin vector from the north pole of the Bloch sphere is smaller than the level of fluctuations, the seeding of the superradiant decay is still dominated by fluctuations. As a consequence, the time $t_{\max}$ to reach maximum gain becomes independent of the signal angle ϕ for sufficiently small ϕ [as shown in Eq. (7) of the main text] and it depends only on the collective decay rate Γ and the number of spins N [as shown in Fig. 2(a) of the main text]. Quantum metrology protocols operate in this regime, $\phi \ll 1$. Figure 2(a) shows how $t_{\max}$ ultimately becomes ϕ dependent and decreases to zero as ϕ increases.

In the regime where $t_{\max}$ is independent of ϕ, the maximum gain $G_{\max}$ defined in Eq. (10) of the main text is also independent of ϕ. This is important because it establishes a simple linear relation between the amplified signal and the initial small value of ϕ after a constant amplification time $t_{\max}$. For larger values of ϕ, $G_{\max}$ decreases as a function of ϕ, as sketched in the inset of Fig. 2(b). The dynamic range of an amplifier quantifies the range of ϕ values over which $G_{\max}$ is constant and a linear amplification relation is obtained. We determine the dynamic range of the spin amplifier numerically by rescaling the gain $G_{\max}(\phi)$ to the range $[0,1]$ by defining

$$\delta G_{\max}(\phi) = \frac{G_{\max}(\phi=0) - G_{\max}(\phi)}{G_{\max}(\phi=0) - 1}$$

and numerically finding the angle $\phi_{-3\mathrm{dB}}$ where $1 - \delta G_{\max}(\phi)$ has decreased to $1/2$. The dynamic range $\phi_{-3\mathrm{dB}}$ is plotted in the main panel of Fig. 2(b).

B. Calibration of $t_{\max}$ and $G_{\max}$

Note that precise knowledge of the number N of spins is *not* required to calibrate the maximum amplification time $t_{\max}$ and the maximum gain $G_{\max}$. Instead, these quantities can be experimentally determined by the following measurement: The spin system is repeatedly prepared in a coherent spin state in the y-z plane, which is tilted away from the z axis by a small angle $\phi < \phi_{-3\mathrm{dB}}$. This can be achieved by standard control pulses. One then switches on the superradiant decay for different time delays t and measures the final transverse S_y polarization. In this way, one maps out $S_y(t)$ as a function of time, which allows one to determine the time-dependent gain $G(t)$ defined in Eq. (10) of the main text [see Fig. 1(b) of the main text]. From this emasurement, one can determine $t_{\max}$ and $G_{\max}$.

C. Analysis of timing errors in the amplification step

The amplification step of the modified Ramsey sequence shown in Fig. 1(a) of the main text requires time-dependent control of the collective decay rate $\Gamma(t)$. Both

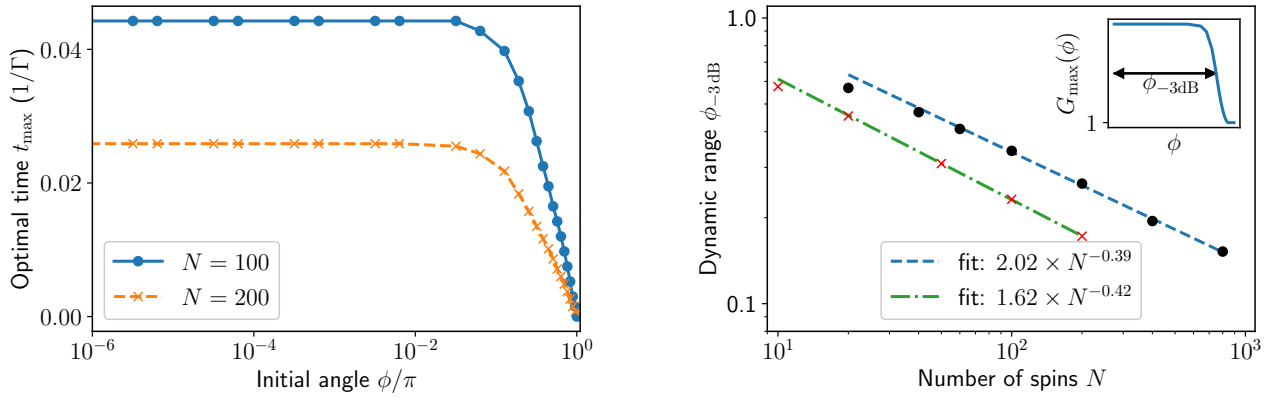

FIG. 2. (a) Time $t_{\max}$ to reach maximum gain as a function of the initial tilt angle ϕ away from the north pole of the collective Bloch sphere, obtained by a numerically exact integration of Eq. (3) of the main text for $\Gamma = 1$ and $\gamma_{\mathrm{rel}} = 0$. In the limit $\phi \to 0$, $t_{\max}$ tends towards a constant value given by Eq. (7) of the main text. (b) Scaling of the dynamic range $\phi_{-3\mathrm{dB}}$ (see Sec. II A for a definition) with the number of spins N for the dissipative spin amplification scheme (black circles and dashed blue fit line) and the OAT-twist-untwist amplification scheme (red crosses and dash-dotted green fit line). The two data points with smallest N have been excluded from the fit.

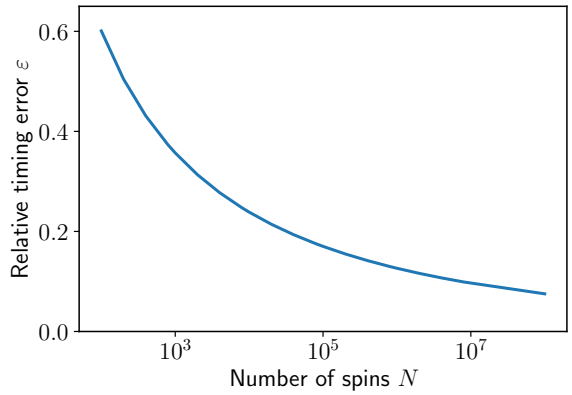

FIG. 3. Maximum relative timing error $\varepsilon = \delta t/t_{\max}$ given in Eq. (8) with the number of spins N. For a relative timing error below the blue line, the uncertainty $(\mathbf{\Delta}\phi)^2_{\delta t}$ due to imperfect control of the amplification time $t_{\max}$ is smaller than the uncertainty due to spin-projection noise.

the optimal amplification time $t_{\max}$ and the FWHM of the gain peak decrease with increasing N, as shown in Figs. 2(a) and (b) of the main text, respectively. Therefore, one may worry that timing errors in the control of $\Gamma(t)$ could limit the performance of our scheme. This is not the case.

Timing errors will contribute an additional term to the uncertainty budget in Eq. (1) of the main text, which can be estimated using mean-field theory. Using Eq. (8) of the main text, we find in the limit $N \gg 1$

$$G(t_{\max} + \delta t) \approx G(t_{\max}) \left[1 - \frac{\Gamma^2}{8} N^2 \delta t^2\right] ,$$

i.e., we are insensitive to timing fluctuations δt to first order in δt, but they decrease the gain quadratically. The corresponding uncertainty in the estimation of ϕ is

$$(\mathbf{\Delta}\phi)^2_{\delta t} = \left(-\frac{\phi}{G(t_{\max})} \frac{\mathrm{d}G}{\mathrm{d}\delta t}\right)^2 = \phi^2 \frac{N^4\Gamma^4}{64} \delta t^4 ,$$

and the overall uncertainty is

$$(\mathbf{\Delta}\phi)^2 = \frac{1 + \sigma^2_{\mathrm{add}}}{N} + \phi^2 \frac{N^4\Gamma^4}{64} \delta t^4 + \frac{\Xi^2_{\mathrm{det}}}{G(t_{\max})^2 N} .$$

The third, detection-noise term can be ignored if N and, thus, $G(t_{\max})$ are large enough. The second, timing fluctuations term vanishes in the metrologically relevant limit $\phi \to 0$.

As a worst-case estimate, we will now assume that ϕ does not vanish but is given by the dynamic range of the amplifier discussed in Sec. II A, $\phi \approx 1/N^{0.4}$. From Fig. 2(a) of the main text, we know that one must be able to switch $\Gamma(t)$ on a timescale $t_{\max} \propto \ln(N)/\Gamma N$. Assuming there is a relative error ε in the timing, $\delta t = \varepsilon t_{\max}$, the overall uncertainty can be rewritten as

$$(\mathbf{\Delta}\phi)^2 \approx \frac{1 + \sigma^2_{\mathrm{add}}}{N} + \frac{1}{N^{0.8}} \frac{\ln^4(N)}{64} \varepsilon^4 .$$

The first, projection-noise term dominates if the relative timing error satisfies

$$\varepsilon \lesssim \sqrt[4]{\frac{64(1 + \sigma^2_{\mathrm{add}}) N^{0.8}}{N \ln^4(N)}} , \tag{8}$$

which puts very moderate requirements on the timing error, as shown in Fig. 3.

D. Impact of the signal field during the amplification step

In the idealized protocol shown in Fig. 1(a) of the main text, the signal is imprinted to the sensing state only during the signal acquisition interval from t_1 to t_2, and it is switched off during the subsequent amplification step from t_2 to t_3. In practice, it may not be possible to switch off the signal. Therefore, we consider a modified quantum master equation

$$\frac{\mathrm{d}}{\mathrm{d}t}\hat{\rho} = -i\left[\omega_{\mathrm{sig}}\hat{S}_z, \hat{\rho}\right] + \Gamma\mathcal{D}[\hat{S}_-]\hat{\rho} \ ,$$

where the Hamiltonian $\hat{H} = \omega_{\mathrm{sig}}\hat{S}_z$ represents the collective rotation about the z axis due to the signal to be sensed. The effect of the (unknown) signal can be gauged away by switching to a rotating frame $\hat{\chi}(t) = e^{i\omega_{\mathrm{sig}}t\hat{S}_z}\hat{\rho}(t)e^{-i\omega_{\mathrm{sig}}t\hat{S}_z}$, in which we recover the pure superradiant decay dynamics described by Eq. (3) of the main text (for $\gamma_{\mathrm{rel}} = 0$),

$$\frac{\mathrm{d}}{\mathrm{d}t}\hat{\chi} = \Gamma\mathcal{D}[\hat{S}_-]\hat{\chi} \ .$$

Maximum gain G_{max} and the corresponding amplification time t_{max} are thus unaffected by the presence of the signal. However, the final state in the lab frame after the amplfication step will be rotated by an angle $\phi_{\mathrm{sig}} = \omega_{\mathrm{sig}}t_{\mathrm{max}}$ as compared to the unperturbed dynamics,

$$\hat{\rho}(t_{\mathrm{max}}) = e^{-i\omega_{\mathrm{sig}}t_{\mathrm{max}}\hat{S}_z}\hat{\chi}(t_{\mathrm{max}})e^{+i\omega_{\mathrm{sig}}t_{\mathrm{max}}\hat{S}_z} \ .$$

Its collective spin vector will be rotated in the equatorial plane away from the y axis by an angle ϕ_{max}.

In the typical quantum metrology setting, the precession frequency is very small, $\omega_{\mathrm{sig}} \to 0$, and the additional rotation during the amplification step can be ignored since $\phi_{\mathrm{sig}} \ll 1$. In particular, for our scheme, the amplification time *decreases* if the number of spins is increased, $t_{\mathrm{max}} \propto \ln(N)/N \approx 1/N$, which suppresses ϕ_{sig} even more.

Note that, even if ϕ_{sig} was not negligible, it could be easily determined by repeating the protocol shown in Fig. 1(a) of the main text twice, measuring $S_x(t_{\mathrm{max}}) \propto \sin(\phi_{\mathrm{sig}})$ and $S_y(t_{\mathrm{max}}) \propto \cos(\phi_{\mathrm{sig}})$ in the two runs, respectively.

III. MEAN-FIELD THEORY IN THE LIMIT OF AN UNDAMPED CAVITY

As discussed in the main text, amplification can also be achieved in a regime where the cavity degree of freedom cannot be eliminated adiabatically, i.e., $\sqrt{N}g \gg \kappa$. In this section, we use MFT to analyze the coherent limit of Eq. (31) of the main text (i.e., $\kappa \to 0$). MFT lets us explore substantially larger system sizes than direct numerical simulation of the Schrödinger equation (which were used to generate the data shown in Fig. 9 of the main text). We consider the resonant ($\omega_{\mathrm{cav}} = \omega$) Tavis-Cummings Hamiltonian (35) of the main text, which reads in a frame rotating at the cavity frequency

$$\hat{H}_{\mathrm{TC}} = g\left(\hat{a}^\dagger\hat{S}_- + \hat{a}\hat{S}_+\right) \ , \tag{9}$$

and we consider a separable initial state consisting of the cavity mode in a vacuum, and the spins maximally polarized in a state $e^{i\phi\hat{S}_x}|\uparrow\ldots\uparrow\rangle$. Using a second-order cumulant expansion [2], we can derive a closed set of equations of motion (EOMs) for the spin-cavity system. Introducing the cavity quadrature operators $\hat{Q} = \left(\hat{a}^\dagger + \hat{a}\right)/\sqrt{2}$, and $\hat{P} = i\left(\hat{a}^\dagger - \hat{a}\right)/\sqrt{2}$ as well as the notation $Q = \langle\hat{Q}\rangle$, $C_{Px} = \langle(\hat{P}\hat{S}_x + \hat{S}_x\hat{P})\rangle/2 - \langle\hat{P}\rangle\langle\hat{S}_x\rangle$, etc., we can readily write down the set of MFT equations of motion:

$$\dot{Q} = -\sqrt{2}gS_y \ , \tag{10}$$
$$\dot{S}_y = -\sqrt{2}g\left(C_{Qz} + S_zQ\right) \ , \tag{11}$$
$$\dot{S}_z = +\sqrt{2}g\left(C_{Px} + C_{Qy} + S_yQ\right) \ , \tag{12}$$
$$\dot{C}_{QQ} = -2\sqrt{2}gC_{Qy} \ , \tag{13}$$
$$\dot{C}_{Qy} = -\sqrt{2}g\left(C_{Qz}Q + C_{QQ}S_z + C_{yy}\right) \ , \tag{14}$$
$$\dot{C}_{Qz} = +\sqrt{2}g\left(C_{Qy}Q + C_{QQ}S_y - C_{yz}\right) \ , \tag{15}$$
$$\dot{C}_{PP} = -2\sqrt{2}gC_{Px} \ , \tag{16}$$
$$\dot{C}_{Px} = -\sqrt{2}g\left(C_{PP}S_z + C_{xx}\right) \ , \tag{17}$$
$$\dot{C}_{xx} = -2\sqrt{2}gC_{Px}S_z \ , \tag{18}$$
$$\dot{C}_{yy} = -2\sqrt{2}g\left(C_{yz}Q + C_{Qy}S_z\right) \ , \tag{19}$$
$$\dot{C}_{yz} = \sqrt{2}g\left[C_{Qy}S_y + \left(C_{yy} - C_{zz}\right)Q - C_{Qz}S_z\right] \ , \tag{20}$$
$$\dot{C}_{zz} = 2\sqrt{2}g\left(C_{yz}Q + C_{Qz}S_y\right) \ . \tag{21}$$

All expectation values (within the second-order cumulant expansion approximation) which are not explicitly shown above have only a trivial evolution, i.e., they remain zero. As an aside, we note that there are two constraints that are also satisfied by our system. The first one is total-angular-momentum conservation, which lets us write

$$S_x^2 + C_{xx} + S_y^2 + C_{yy} + S_z^2 + C_{zz} = \frac{N}{2}\left(\frac{N}{2} + 1\right) \ , \tag{22}$$

and the second one is conservation of the total excitation number, which yields

$$\frac{1}{2}\left(C_{QQ} + Q^2 + C_{PP} + P^2 - 1\right) + S_z = \frac{N}{2} \ . \tag{23}$$

Either (or both) of the above constraints could be used to further reduce the full set of EOMs shown above.

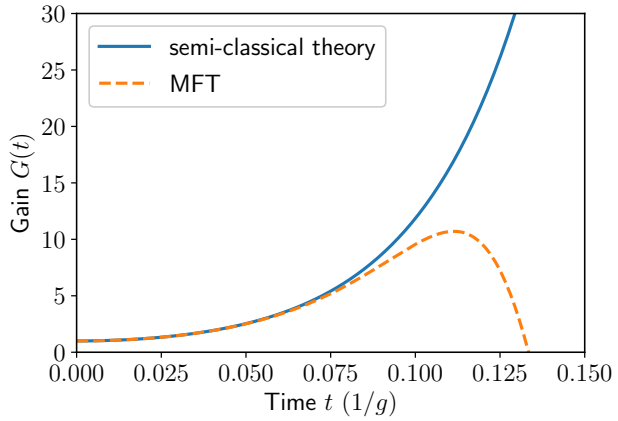

FIG. 4. Comparison between mean-field theory and a semiclassical approximation of the amplification dynamics. Gain as a function of time obtained from MFT (given by Eqs. (10) to (21)) as well as a semiclassical approximation (given by Eqs. (27) to (28)) for $N = 1000$. The semiclassical approximation cannot be used to properly describe the evolution of the cavity-spin system.

A. Scaling of the gain

Solving the system of equations (10) to (21) numerically, we can study the scaling of the maximum gain $G_{\max}$ as well as the the corresponding time scale $t_{\max}$ for systems with very large spin number N, a regime which is inaccessible by numerical integration of the Schrödinger equation. Figure 1(a) shows the scaling of $G_{\max}$, while panel (b) displays the corresponding time $t_{\max}$ required to reach the optimal gain value, both as a function of spin number N. We observe scaling behavior that very closely resembles the one observed for smaller-N Schrödinger-equation simulations shown in Fig. 9 of the main text. Like in the dissipative version of our amplification protocol, the gain scales $\propto \sqrt{N}$, while $t_{\max}$ has a parametrically slower N-scaling, $t_{\max} \propto \ln \sqrt{N}/\sqrt{N}$.

B. Semi-classical theory

Following work in [3], one might hope that much of the core physics or the amplification in the coherent limit of our amplification protocol could be captured by a semiclassical approximation, where all fluctuations (i.e., the covariances) are neglected. Such a case would let us simplify the set of Eqs. (10) to (21) to

$$\dot{Q} = -\sqrt{2}gS_y \ , \tag{24}$$

$$\dot{S}_y = -\sqrt{2}gS_zQ \ , \tag{25}$$

$$\dot{S}_z = +\sqrt{2}gS_yQ \ , \tag{26}$$

which, using Eq. (23) could be further reduced to

$$\dot{Q} = -\sqrt{2}gS_y \ , \tag{27}$$

$$\dot{S}_y = -\sqrt{2}g\left(\frac{N}{2} - \frac{1}{2}\left(Q^2 - 1\right)\right)Q \ . \tag{28}$$

These semiclassical equations indeed predict that S_y will grow at short time. However, solving Eqs. (27) and (28) numerically, one finds that S_y increases monotonically over a time scale much longer than $t_{\max}$ obtained from MFT, see Fig. 4. Therefore, it is clear that one must include the effects of fluctuations to properly describe the amplification physics in the coherent $\kappa \to 0$ limit.

IV. ADDED NOISE σ^2_{add} IN THE LIMIT OF AN UNDAMPED CAVITY

Above, we gave a heuristic argument (assuming linear amplification dynamics) which showed that the added noise σ^2_{add} (defined in Eq. (13) of the main text), should approximately follow the relation

$$\sigma^2_{\text{add}} \geq 1 - \frac{1}{G^2_{\max}N} \tag{29}$$

in the limit of large spin number N. For dissipative amplification, we found numerically that the added noise stays close to this heuristic expectation and tends to $\sigma^2_{\text{add}} \approx 1.3$ in the large-N limit (see Fig. 3(b) of the main text). Here, we show that similar behavior is also present in the case of purely coherent evolution, where $\kappa \to 0$. Specifically, Fig. 5 shows σ^2_{add} as a function of spin number N. Black dots correspond to data obtained from solving the Schrödinger equation numerically, while the dashed blue line indicates $1 - 1/G^2_{\max}N$. Curiously, we see similar behavior to the dissipative case and observe $\sigma^2_{\text{add}} \lesssim 1.3$ in the large-N limit. Consequently, our amplification protocol could also be useful in the coherent limit if the readout noise is not extremely large and one cares about approaching the SQL.

V. COMPARISON BETWEEN SEMICLASSICAL AND MEAN-FIELD-THEORY DYNAMICS OF THE TRANSVERSE MAGNETIZATION

In this section, we briefly discuss the effect of radiation damping in NMR systems [4] (which is somewhat related to superradiance) and we show why our dissipative amplification scheme is very different from sensing protocols based on radiation damping [5, 6].

In NMR setups, the time-dependent magnetic field $\vec{M} = (M_x, M_y, M_z)$ of a spin vector precessing about the quantization axis (typically the z axis) induces a current in the measurement coil. This current generates a magnetic field which aims to rotate the spin vector back to its stable equilibrium position. This process is called radiation damping [4] and can be described by classical Bloch

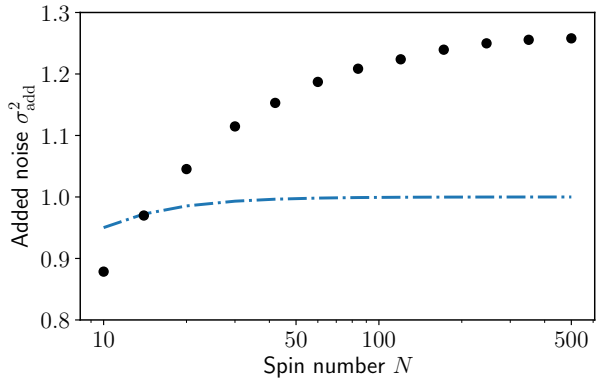

FIG. 5. Added noise $\sigma^2_{\rm add}$ in the coherent spin-amplification protocol, calculated by numerical integration of the Schrödinger equation using the resonant Tavis-Cummings Hamiltonian given in Eq. (35) of the main text with $\omega_{\rm cav} = \omega$. The quantity $\sigma^2_{\rm add}$ at the optimal evolution time $t_{\rm max}$ (data points) is close to the amount of noise $1 - 1/G^2_{\rm max}N$ that is expected based on a heuristic argument valid in the limit $N \gg 1$ (dashed-dotted line).

equations

$$\frac{\mathrm{d}}{\mathrm{d}t}M_{x,y} = -\gamma M_z M_{x,y} - \frac{1}{T_2}M_{x,y}\ , \tag{30}$$

$$\frac{\mathrm{d}}{\mathrm{d}t}M_z = +\gamma(M_x^2 + M_y^2) - \frac{1}{T_1}\left(M_z - \frac{N}{2}\right)\ , \tag{31}$$

where T_1 and T_2 are the relaxation and dephasing time, respectively, and γ is the gyromagnetic ratio of the spins. These equations are similar to the *semiclassical* equations of motion for superradiant decay [7], which can be obtained from Eq. (21) of the main text by deriving the equations of motion for $S_k \equiv \langle \hat{S}_k \rangle$, $k \in \{x, y, z\}$, and factorizing all higher-order expectation values $\langle \hat{S}_j \hat{S}_k \rangle \approx \langle \hat{S}_j \rangle \langle \hat{S}_k \rangle$,

$$\frac{\mathrm{d}}{\mathrm{d}t}S_{x,y} = +\Gamma S_z S_{x,y} - \left(\frac{\Gamma}{2} + \gamma_\phi + \frac{\gamma_{\rm rel}}{2}\right)S_{x,y}\ , \tag{32}$$

$$\frac{\mathrm{d}}{\mathrm{d}t}S_z = -\Gamma\left(S_x^2 + S_y^2\right) - \Gamma S_z - \gamma_{\rm rel}\left(S_z + \frac{N}{2}\right)\ . \tag{33}$$

Note that the two sets of differential equations have opposite stable steady-state solutions: $M_{x,y}(t \to \infty) = 0$ and $M_z(t \to \infty) = +N/2$ as opposed to $S_{x,y}(t \to \infty) = 0$ and $S_z(t \to \infty) = -N/2$.

For $S_z(0) \approx N/2 \gg 1/2$ one can neglect the term $-\Gamma S_{x,y}/2$ in Eq. (32) at short times. In the absence of local relaxation and dephasing, $\gamma_{\rm rel}, \gamma_\phi \to 0$ and $T_1, T_2 \to \infty$, one then finds that Eqs. (30) and (31) are identical to Eqs. (32) and (33) upon the substitution $M_k \to S_k$, except for the second term $-\Gamma S_z$ in Eq. (33). This term captures spontaneous decay and is crucial to "seed" the superradiant decay dynamics out of a perfectly inverted state. Since is not present in the radiation damping equation (31), a magnetization aligned exactly along the $+z$ or $-z$ direction is a stable solution of Eqs. (30) and (31) in the absence of T_1 relaxation. Seeding of the radiation damping dynamics must be introduced manually by considering thermal fluctuations of the current in the pickup coil [5], experimental imperfections which cause a small deviations from a perfectly inverted state [5], and dipole-dipole interactions between the spins [8]. These effects will cause the magnetization to ultimately flip back to the stable orientation along the $+z$ direction and lead to a large transient magnetization in the x-y plane, similar to a superradiant emission burst.

Walls *et al.* proposed to use the time delay of this peak in the transverse magnetization for sensing [6]. They consider a system consisting of a solute in solution. The solvent spins are initialized in the metastable state, i.e., they are antialigned with the external magnetic field. The initial transverse magnetization of the solute spins triggers the solvent spins to flip back to the stable state. If the solute's magnetization is larger than the scale of the fluctuations around the metastable state, the delay time depends on the magnitude of the solute's initial magnetization [5, 6]. For a smaller solute magnetization, the delay time becomes independent of the state of the solvent spins and the radiation-damping-based scheme becomes insensitive.

In our scheme, such a situation would correspond to an initial tilt angle ϕ larger than the fluctuations of the sensing state. While one could in principle reduce the level of thermal fluctuations by cooling the setup, unavoidable quantum fluctuations of the sensing state will pose a strict lower bound on the minimum detectable angle ϕ in the quantum sensor. However, quantum metrology protocols do operate in the regime where the angle ϕ is much *smaller* than the scale of the quantum or thermal fluctuations. In this regime, the delay time is *independent* of ϕ [as shown in Eq. (7) of the main text] and, thus, the radiation-damping-based amplification scheme is useless for quantum metrology.

Instead of focusing on the delay time, our scheme measures the amplitude of the transverse magnetization peak, which remains sensitive to the initial tilt angle ϕ [as shown in Eq. (9) of the main text]. We stress that this amplitude dynamics *cannot* be generated by the classical backaction due to radiation damping. Figure 6 compares the decay dynamics due to radiation damping, the semiclassical equations of motion for superradiant decay, the mean-field theory for superradiant decay given by Eqs. (B2) to (B6) of the main text, and results obtained by numerically exact integration of the quantum master equation (21) of superradiant decay. As expected from the above discussion, the Bloch equations of radiation damping and the semiclassical equations of motion for superradiance predict very similar dynamics. While they manage to capture the dynamics of the z component of the magnetization qualitatively, they fail completely to describe the dynamics of the transverse magnetiation in the x-y plane, which is at the heart of our spin amplification scheme. This is due to the fact that Eqs. (30)

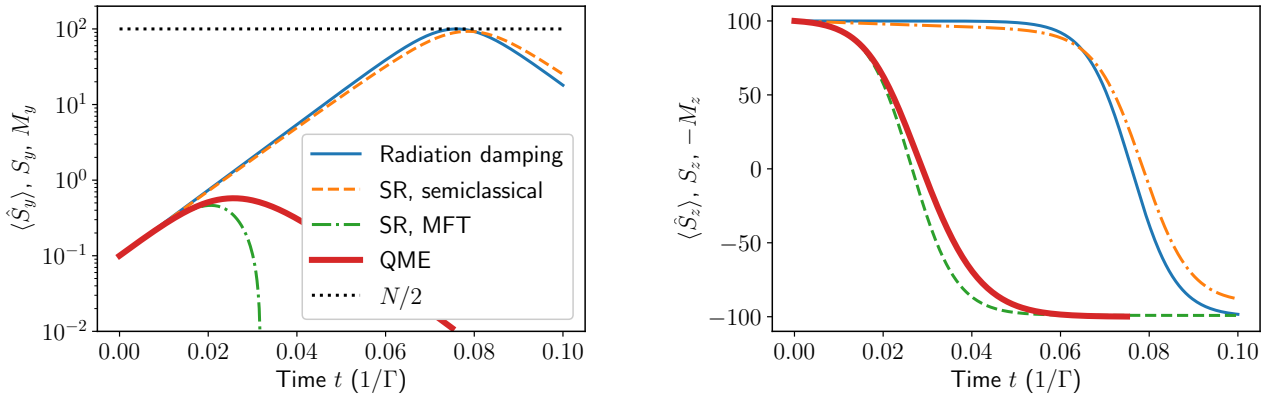

FIG. 6. (a) y magnetization and (b) z magnetization for radiation damping [Eqs. (30) and (31)], a semiclassical treatment of superradiance (SR) [Eqs. (32) and (33)], a mean-field treatment of superradiance [Eqs. (B2) to (B6)], and an numerically exact solution of the quantum master equation (QME) Eq. (21). The parameters are $N = 200$, $\Gamma = \gamma = 1$, $\gamma_\phi = \gamma_{\rm rel} = 0$ and $T_1, T_2 \to \infty$. The initial state is a coherent spin state in the z-y plane tilted away from a perfectly inverted state (i.e., a state pointing along the $+z$ direction for superradiance, along the $-z$ direction for radiation damping) by an angle $\phi = 0.001$. While all methods describe the dynamics of the z magnetization qualitatively correctly, radiation damping and a semiclassical treatment of superradiance fail to describe the dynamics of the y magnetization correctly and predict a maximum transverse magnetization of $N/2$ (dotted black line). The same is true in the case of a unitary Tavis-Cummings interaction, discussed in Sec. III and shown in Fig. 4.

and (31) preserve the length of the magnetization vector (for $T_1, T_2 \to \infty$) and, thus, describe a *rotation* of a *pure state* on the surface of the collective Bloch sphere. Superradiant decay, however, creates a highly *mixed* state at transient times, whose spin vector is in the interior of the Bloch sphere. In order to describe the transverse amplitude dynamics of superradiant decay, one must use at least a MFT approach, which takes quantum correlations into account.

In conclusion, while radiation damping in NMR has some similarity with a semiclassical analysis of superradiance, it leads to a completely different transient dynamics of the x-y magnetization. Therefore, it cannot be used to implement our spin-amplification scheme. While radiation damping dynamics could be used to infer a sufficiently strong initial transverse magnetization in NMR more efficiently from the peak delay time than from a direct measurement [6] it cannot be used in the context of quantum metrology. In contrast, our scheme is compatible with a standard quantum-metrology Ramsey sequence and allows one to approach the SQL even in the presence of extremely large readout noise, which is an aspect that has not been analyzed in the context of NMR.

VI. OAT AMPLIFICATION WITH SINGLE-SPIN DISSIPATION USING MEAN-FIELD THEORY

In the main text we showed that the performance of the OAT amplification protocol is particularly sensitive to noise, both collective decay (governed by the cavity relaxation rate κ) as well as single-spin dephasing and single-spin relaxation (governed by the rates γ_ϕ and $\gamma_{\rm rel}$ respectively). Here, we present additional results obtained using MFT simulations, which explore this effect in more detail.

As discussed in the main text, collective decay generates a large background that needs to be subtracted to extract the amplified signal. Therefore, we consider the gain $G_{\rm sub}^{\rm OAT}(t)$ defined in Eq. (42) of the main text, which is the signal after background subtraction, $\delta\langle \hat{S}_y(t) \rangle = \langle \hat{S}_y(t,\phi) \rangle - \langle \hat{S}_y(t,0) \rangle$, normalized to the initial signal $\langle \hat{S}_z \rangle = N\phi/2$. Single-spin decay decreases the gain over time and therefore limits the maximum possible amplification time. To determine the maximum gain, one thus has to optimize both the detuning (which determines the ratio between the OAT strength χ and the collective decay rate Γ, see main text), and the amplification time $t_{\rm max}$. The result of this optimization is shown in Fig. 7, where we compare $G_{\rm sub}^{\rm OAT}(t)$ to its ideal value obtained in the limit $\eta_k \to \infty$ (i.e., no local dissipation). The gain in this limit is equivalent to the gain in the absence of any dissipation, since the condition $\Delta_{\rm opt} \gg \kappa$ holds, i.e., collective dissipation is strongly suppressed. Similar to Fig. 10(a) of the main text, we evaluate the maximum gain at the time $t_{\rm max} = \tau_1$ of the first peak of $G_{\rm sub}^{\rm OAT}(t)$. Figures 7(a) and (b) show data for single-spin dephasing and single-spin relaxation, respectively, and the insets show the corresponding values of the optimal spin-cavity detuning $\Delta_{\rm opt}$. In both scenarios, very high *single-spin* cooperativities are required to result signifi-

cant gain: one needs $\eta_\phi \gg \sqrt{N}$ and $\eta_{\rm rel} \gg N^{0.9}$.

VII. MORE GENERAL MODEL OF THE READOUT PROCESS

In this section, we provide an alternative derivation of the readout model. In contrast to the discussion in App. A of the main text, we consider a more generic situation where the overall measurement result $n \equiv \sum_{j=1}^N n_j$ is the sum of N independent random measurement results n_j which are collected in parallel from each spin. The probability distribution $\mathcal{P}_{\sigma_j}(n_j)$ of each individual result n_j depends on the quantum state of the corresponding spin j in the measurement basis $|\sigma_j\rangle$. In contrast to App. A, we leave the measurement basis and the properties of the probability distribution $\mathcal{P}_{\sigma_j}(n_j)$ completely general for now, and we will only specialize the final result to the case of fluorescence readout. Moreover, we do not use the language of POVMs, since the addition of readout noise is a classical process and a POVM is not necessarily needed to model it.

For a general pure single-spin state $|\psi_j\rangle = \sum_{\sigma_j} c_{\sigma_j}|\sigma_j\rangle$, we assume that the measurement result n_j will be distributed according to the weighted sum of the probability distributions of the corresponding basis states, $\mathcal{P}_{|\psi_j\rangle}(n_j) = \sum_{\sigma_j} |c_{\sigma_j}|^2 \mathcal{P}_{\sigma_j}(n_j)$. Given an ensemble of N spins, the probability distribution of the overall measurement result $n = \sum_{j=1}^N n_j$ for a product state $|\sigma_1, \ldots, \sigma_N\rangle$ in the measurement basis is the convolution of all single-spin probability distributions, $\mathcal{P}_{\sigma_1,\ldots,\sigma_N}(n) = \left(*_{j=1}^N \mathcal{P}_{\sigma_j}\right)(n)$. Similar to the single-spin case, we assume that the probability distribution of n for a general pure N-spin state

$$|\psi\rangle = \sum_{\{\sigma_j\}} c_{\sigma_1,\ldots,\sigma_N} |\sigma_1, \ldots, \sigma_N\rangle \tag{34}$$

is given by the average

$$\mathcal{P}_{|\psi\rangle}(n) = \sum_{\{\sigma_j\}} |c_{\sigma_1,\ldots,\sigma_N}|^2 \mathcal{P}_{\sigma_1,\ldots,\sigma_N}(n) \ . \tag{35}$$

We are now interested in the fluctuations of n with respect to the probability distribution (35),

$$\begin{aligned}(\boldsymbol{\Delta} n)^2 &\equiv \sum_n n^2 \mathcal{P}_{|\psi\rangle}(n) - \Big(\sum_n n \mathcal{P}_{|\psi\rangle}(n)\Big)^2 \\ &= \sum_n \sum_{\{\sigma_j\}} n^2 |c_{\sigma_1,\ldots,\sigma_N}|^2 \mathcal{P}_{\sigma_1,\ldots,\sigma_N}(n) \\ &\quad - \Big(\sum_n \sum_{\{\sigma_j\}} n |c_{\sigma_1,\ldots,\sigma_N}|^2 \mathcal{P}_{\sigma_1,\ldots,\sigma_N}(n)\Big)^2 \ . \end{aligned} \tag{36}$$

The second line shows that calculating a moment n^m of the probability distribution (35) involves two different averages: First, a n-average with respect to the classical conditional probability distribution $\mathcal{P}_{\sigma_1,\ldots,\sigma_N}(n)$ describing the readout for a particular spin configuration $\{\sigma_j\}$ in the measurement basis. We will denote this average by

$$\mathbf{E}_{\{\sigma_j\}}[n^m] \equiv \sum_n n^m \mathcal{P}_{\sigma_1,\ldots,\sigma_N}(n) \ . \tag{37}$$

Second, an average of the classical expectation values $\mathbf{E}_{\{\sigma_j\}}[n^m]$ with respect to the probabilities $|c_{\sigma_1,\ldots,\sigma_N}|^2$ to obtain a certain spin configuration $\{\sigma_j\}$ in the quantum state (34). This is the step where the properties of the quantum state $|\psi\rangle$ enter and we will denote this average by

$$\langle f_{\{\sigma_j\}} \rangle_{|\psi\rangle} \equiv \sum_{\{\sigma_j\}} |c_{\sigma_1,\ldots,\sigma_N}|^2 f_{\{\sigma_j\}} \ , \tag{38}$$

where $f_{\{\sigma_j\}}$ is a function that depends on the spin configuration $\{\sigma_j\}$. Note that this does not look like the typical quantum expectation value of an observable with respect to the quantum state $|\psi\rangle$. However, for a specific readout model, the moments of the probability distribution $\mathcal{P}_{\sigma_1,\ldots,\sigma_N}(n)$ will be related to moments of an observable of the quantums state: for instance, in the case of fluorescence readout discussed below, this will be the spin component $\hat{S}_z$ [see also Eq. (A4) of the main text]. Therefore, the expectation value $\langle f_{\{\sigma_j\}} \rangle_{|\psi\rangle}$ will turn into a familiar quantum expectation value.

With these definitions at hand, the variance of n given by Eq. (36) can be rewritten as follows:

$$\begin{aligned}(\boldsymbol{\Delta} n)^2 &= \langle \mathbf{E}_{\{\sigma_j\}}[n^2] \rangle_{|\psi\rangle} - \langle \mathbf{E}_{\{\sigma_j\}}[n] \rangle_{|\psi\rangle}^2 \\ &= \Big(\langle \mathbf{E}_{\{\sigma_j\}}[n^2] \rangle_{|\psi\rangle} - \langle \mathbf{E}_{\{\sigma_j\}}[n]^2 \rangle_{|\psi\rangle} \Big) \\ &\quad + \Big(\langle \mathbf{E}_{\{\sigma_j\}}[n]^2 \rangle_{|\psi\rangle} - \langle \mathbf{E}_{\{\sigma_j\}}[n] \rangle_{|\psi\rangle}^2 \Big) \ , \end{aligned} \tag{39}$$

where we added a zero in the last line. Similar to Eq. (A5) of the main text, the first term in Eq. (39) describes the classical noise which is added by the detector due to the fact that $\mathcal{P}_{\sigma_1,\ldots,\sigma_N}(n)$ has a finite variance for each basis state $|\sigma_1, \ldots, \sigma_N\rangle$. The second term represents the variance of $\mathbf{E}_{\{\sigma_j\}}[n]$ due to the intrinsic fluctuations of the state $|\psi\rangle$, i.e., its intrinsic spin-projection noise expressed in terms of the measured quantity n.

The average measurement result can be expressed as follows:

$$\bar{n} \equiv \sum_n n \mathcal{P}_{|\psi\rangle}(n) = \langle \mathbf{E}_{\{\sigma_j\}}[n] \rangle_{|\psi\rangle} \ . \tag{40}$$

The change of $\bar{n}$ with respect to the signal ϕ, $\partial_\phi \bar{n}$, is the transduction factor that we need to refer the measure-

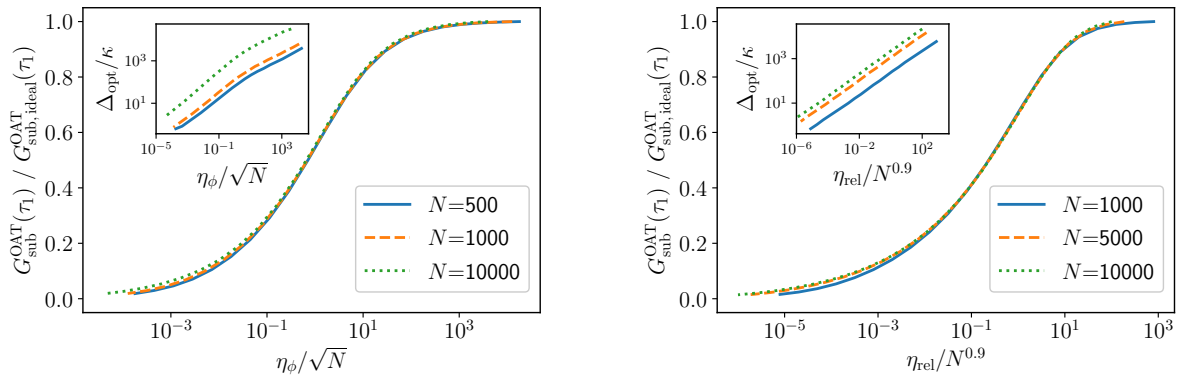

FIG. 7. Performance of the OAT spin amplification protocol proposed in Ref. [9] in the presence of **(a)** single-spin dephasing and **(b)** single-spin relaxation. Each plot shows the optimal gain $G^{\rm OAT}_{\rm sub}(t)$ after background subtraction (evaluated at the time τ_1 of the first peak) as a function of the single-spin cooperativity η_k (with $k = \{\phi, \mathrm{rel}\}$), normalized to the gain calculated in the limit $\eta_k \to \infty$. Simulations were done using MFT for $N = 1000$, 5000, and 10000 spins, and the spin-cavity detuning was optimized for each value of η_k (see insets). These plots suggest that, to achieve significant performance, the *single-spin* cooperativity must be substantially large and satisfy $\eta_\phi \gg \sqrt{N}$ and $\eta_{\rm rel} \gg N^{0.9}$.

ment error $(\mathbf{\Delta}n)^2$ back to the signal:

$$(\mathbf{\Delta}\phi)^2 = \frac{(\mathbf{\Delta}n)^2}{|\partial_\phi \bar{n}|^2} = \frac{\langle \mathbf{E}_{\{\sigma_j\}}[n^2]\rangle_{|\psi\rangle} - \langle \mathbf{E}_{\{\sigma_j\}}[n]^2\rangle_{|\psi\rangle}}{|\partial_\phi \langle \mathbf{E}_{\{\sigma_j\}}[n]\rangle_{|\psi\rangle}|^2} + \frac{\langle \mathbf{E}_{\{\sigma_j\}}[n]^2\rangle_{|\psi\rangle} - \langle \mathbf{E}_{\{\sigma_j\}}[n]\rangle^2_{|\psi\rangle}}{|\partial_\phi \langle \mathbf{E}_{\{\sigma_j\}}[n]\rangle_{|\psi\rangle}|^2} \ . \tag{41}$$

Note that both the numerator and denominator in the second term are expressed using only $\mathbf{E}_{\{\sigma_j\}}[n]$, i.e., if n is related to some spin observable $\hat{O}$ by a linear transformation [e.g., $\hat{S}_z$ as shown in Eq. (A4) of the main text], the conversion factors will drop out and the second term will become the bare spin-projection noise with respect to $\hat{O}$.

Finally, we specialize this result to the case of fluorescence readout [10]. In this case, the quantity n denotes the number of detected photons and $\mathcal{P}_{|\sigma_j\rangle}(n_j)$ is a Poissonian distribution with mean $n_{\rm b}$ ($n_{\rm d}$) if spin j is in the bright (dark) state. The overall measurement result n also follows a Poissonian distribution with expectation value

$$\mathbf{E}_{\{\sigma_j\}}[n] = N_{\rm b} n_{\rm b} + N_{\rm d} n_{\rm d} \ , \tag{42}$$

where $N_{\rm b}$ ($N_{\rm d}$) denotes the number of spins in the bright (dark) state. Using the basis $|j, m\rangle$ of simultaneous eigenstates of $\hat{\mathbf{S}}^2$ and $\hat{S}_z$, one can rewrite the state (34) as $|\psi\rangle = \sum_j \sum_{m=-j}^{j} c_m^j |j, m\rangle$. Assuming the ground state of each spin is the bright state, we then have $N_{\rm b} = N/2 - m$ and $N_{\rm d} = N/2 + m$ and obtain

$$\langle \mathbf{E}_{\{\sigma_j\}}[n]\rangle_{|\psi\rangle} = N n_{\rm avg} \left[1 - \frac{2}{N}\langle \hat{S}_z\rangle \tilde{C}\right] \ , \tag{43}$$

where $n_{\rm avg} = (n_{\rm b} + n_{\rm d})/2$ is the average number of emitted photons and $\tilde{C} = (n_{\rm b} - n_{\rm d})/(n_{\rm b} + n_{\rm d})$ is the contrast between the bright and the dark state [10–12]. Evaluating Eq. (41), we find

$$(\mathbf{\Delta}\phi)^2 = \frac{\frac{N}{4}\frac{1 - 2\tilde{C}\langle \hat{S}_z\rangle/N}{\tilde{C}^2 n_{\rm avg}}}{|\partial_\phi \langle \hat{S}_z\rangle|^2} + \frac{\langle \hat{S}_z^2\rangle - \langle \hat{S}_z\rangle^2}{|\partial_\phi \langle \hat{S}_z\rangle|^2} \ . \tag{44}$$

This is the same result as Eq. (A7) of the main text.

[1] C. M. Caves, Quantum limits on noise in linear amplifiers, Phys. Rev. D **26**, 1817 (1982).
[2] R. Kubo, Generalized cumulant expansion method, Journal of the Physical Society of Japan **17**, 1100 (1962).
[3] J. Keeling, Quantum corrections to the semiclassical collective dynamics in the tavis-cummings model, Phys. Rev. A **79**, 053825 (2009).
[4] N. Bloembergen and R. V. Pound, Radiation damping in magnetic resonance experiments, Phys. Rev. **95**, 8 (1954).
[5] M. P. Augustine, S. D. Bush, and E. L. Hahn, Noise triggering of radiation damping from the inverted state, Chemical Physics Letters **322**, 111 (2000).
[6] J. D. Walls, S. Y. Huang, and Y.-Y. Lin, Spin amplification in solution magnetic resonance using radiation damping, The Journal of Chemical Physics **127**, 054507

(2007).
[7] N. E. Rehler and J. H. Eberly, Superradiance, Phys. Rev. A **3**, 1735 (1971).
[8] V. I. Yukalov, Origin of pure spin superradiance, Phys. Rev. Lett. **75**, 3000 (1995).
[9] E. Davis, G. Bentsen, and M. Schleier-Smith, Approaching the heisenberg limit without single-particle detection, Phys. Rev. Lett. **116**, 053601 (2016).
[10] J. F. Barry, J. M. Schloss, E. Bauch, M. J. Turner, C. A. Hart, L. M. Pham, and R. L. Walsworth, Sensitivity optimization for nv-diamond magnetometry, Rev. Mod. Phys. **92**, 015004 (2020).
[11] J. M. Taylor, P. Cappellaro, L. Childress, L. Jiang, D. Budker, P. R. Hemmer, A. Yacoby, R. Walsworth, and M. D. Lukin, High-sensitivity diamond magnetometer with nanoscale resolution, Nature Physics **4**, 810 (2008).
[12] B. J. Shields, Q. P. Unterreithmeier, N. P. de Leon, H. Park, and M. D. Lukin, Efficient readout of a single spin state in diamond via spin-to-charge conversion, Phys. Rev. Lett. **114**, 136402 (2015).